Journal of Applied Polymer Science

Synergistic Effect of Poly(ethylene glycol) and Graphene Oxides on the Crystallization Behavior of Poly(L-lactide)

Jing-Hui Yang,[1,2] Ying Shen,[1] Wei-Di He,[1] Nan Zhang,[1] Ting Huang,[1] Ji-Hong Zhang,[1] Yong Wang[1]

[1]Key Laboratory of Advanced Technologies of Materials (Ministry of Education), School of Materials Science and Engineering, Southwest Jiaotong University, Erhuan Road, North I, Number 111, Chengdu, Sichuan 610031, China

[2]State Key Laboratory of Polymer Materials Engineering, Sichuan University, Chengdu 610065, China

Correspondence to: J.-H. Yang (E-mail: yangjinghui_84@163.com) or Y. Wang (E-mail: yongwang1976@163.com)

ABSTRACT: In this article, we report the combined effects of poly(ethylene glycol) (PEG) and/or graphene oxides (GOs) on the crystallization behavior of poly(L-lactide) (PLLA) under different crystallization conditions, such as nonisothermal crystallization, isothermal crystallization, and annealing-induced cold crystallization. Differential scanning calorimetry (DSC), wide-angle X-ray diffraction, and polarized optical microscopy were used to study the crystallization kinetics and crystallinity to illustrate the effects of PEG and/or GOs on the crystallization behavior of PLLA. The results show that PEG functioned as a plasticizer and improved the chain mobility of /PLLA during crystallization and the GOs acted as efficient nucleation agents and accelerated the crystallization rate. Finally, both PEG and GOs improved the crystallization ability of PLLA. Importantly, the simultaneous addition of PEG and GOs led to a synergistic effect on the crystallization behavior of PLLA under all conditions. © 2013 Wiley Periodicals, Inc. J. Appl. Polym. Sci. 130: 3498–3508, 2013

KEYWORDS: composites; crystallization; graphene and fullerenes; nanotubes

Received 27 December 2012; accepted 4 April 2013; Published online 24 June 2013

DOI: 10.1002/app.39371

INTRODUCTION

Environmentally friendly polymers have attracted significant interests in recent years. In this field, poly(L-lactide) (PLLA) is one of the most promising candidates because it can not only be derived from agricultural products but also be totally degraded into carbon dioxide and water.[1,2] PLLA is a linear, aliphatic polyester that is mainly used in biomedical and film-packing applications. On the other hand, PLLA has good mechanical properties and thermal plasticity; therefore, PLLA is potentially interesting for various end-use applications in the industrial field. Because PLLA is a semicrystalline polymer, its mechanical and physical properties are governed by its supermolecular structures, which are, in turn, controlled by the crystallization process.[3–5] A reinforcement or improvement of the physical properties is expected when the crystallization behavior of PLLA is changed.

The crystallization behavior of PLLA has been investigated extensively during recent years. A great amount of research has shown it is difficult for PLLA to achieve a high crystallization degree (X_c) during traditional processing, such as extrusion and injection molding, because of the nonisothermal conditions. Thus, the final properties of PLLA, which are strongly dependent on its crystallization behavior, are greatly affected.[6–8] For instance, PLLA with a low crystallinity may exhibit a lower modulus above the glass-transition temperature and poor heat resistance; this limits the application of PLLA in the general plastics use.[9,10] Therefore, it is urgent to seek a new strategy to control the crystallization behavior of PLLA and further realize the enhancement or improvement of its properties.

As we know, two key issues in the crystallization behavior of semicrystalline polymers are the nucleation activation energy and mobility of chain segments. On the basis of these two issues, there are two main categories in the improvement of the crystallization ability of PLLA. On one hand, plasticizers such as oligomeric PLLA,[11] poly(ethylene oxide),[12] thermoplastic starch,[13] and poly(3-hydroxy butyrate)[14] can improve the mobility of polymer chain segments and finally benefit the crystallization of PLLA. The other important category is the introduction of nucleation agents,[6,7] especially some nanofillers such as carbon nanotubes (CNTs),[15,16] layered silicates,[17–19] and whiskers;[20] this is also thought to be the most common way to enhance the heterogeneous crystallization of the crystalline polymer matrix. Nanofillers as nucleation agents can effectively decrease the nucleation activation energy, and thus promote the crystallization of PLLA. Graphene and its derivatives exhibit a two-dimensional (2D) geometry as nanoclays and have sp^2

carbon atoms arranged in a hexagonal lattice as CNTs. More importantly, graphene and its derivatives have also been considered as potential nucleation agents for crystalline polymers.[21,22] Xu et al.[23] compared the geometric effects of both CNTs and graphene nanosheets (GNSs) on the crystallization kinetics of PLLA. As for PLLA/CNT and PLLA/GNS nanocomposites, the crystallization half-time ($t_{1/2}$) was shortened compared with pure PLLA. However, in contrast to PLLA/CNT composites, whose crystallization induction time was decreased with increasing content of CNTs, the crystallization induction time of PLLA/GNS composites showed an inverse trend. Gao et al.[24] and Bao et al.[25] prepared PLLA/graphene nanocomposites by masterbatch methods, and both the crystallinity and crystallization rate were greatly improved. Li et al.[26] investigated the crystallization behavior of polyethylene (PE)/reduced graphene oxide (RGO) composites obtained by solution blending; the results showed that crystallization temperatures (T_c's) shifted to higher temperatures for all of the composites compared with pure PE. This indicated the supercapability of RGO nanosheets to induce the heterogeneous crystallization of PE. Obviously, graphene and its derivatives have emerged as potential candidates for improving crystallization via heterogeneous nucleation in crystalline polymers.

In this study, to improve the crystallization behavior of PLLA, graphene derivative–graphene oxides (GOs), and poly(ethylene glycol) (PEG) were incorporated into the PLLA matrix. First, it was reported that oxidized CNTs showed high-quality dispersion within the PEG matrix because of a lowered tendency of the filler to aggregate; this could be attributed to electrostatic repulsion and/or the improved wettability of the CNT surfaces by the polar polymer chains, which resulted from the surface polarity of the oxidized CNTs.[27] In our previous study,[28] we found that PEG preferred to distribute around functionalized CNTs in PLLA/PEG/CNT composites; this was also ascribed to the good interaction between the PEG and functionalized CNTs. In this case, we expected that water-soluble PEG with a low molecular weight would serve as a dispersive agent to improve the dispersion of GOs in the PLLA matrix so that the well-dispersed GOs in the PLLA matrix could realize a strong nucleation ability. On the other hand, PEG has been proven to be an efficient plasticizer for PLLA to enhance the mobility of polymer chain segments.

Therefore, on the basis of the discovery of new nanofillers, graphene and its derivatives, the first purpose of this study was to explore the nucleation efficiency of GOs. More importantly, this motivated us to study the combined effects of plasticizers (PEG) and nucleation agents (GOs). In this case, more information could be applied to control the crystallization behavior of PLLA. In detail, the crystallization behavior of PLLA/PEG/GO ternary composites under different crystallization conditions, including nonisothermal and isothermal conditions and during the annealing process, was investigated via comparison with PLLA and PLLA/PEG and PLLA/GO composites. We expected to explore an efficient strategy for promoting the PLLA crystallization behavior.

Table I. Sample Notations and Compositions of the Blends

Sample	PLLA (wt %)	PEG (wt %)	GO (wt %)
PLLA	100	—	—
PLLA/GO	99.5	—	0.5
PLLA/PEG	90	10	—
PLLA/PEG/GO	89.5	10	0.5

EXPERIMENTAL

Materials

Graphites with an average particle size of 10–20 μm and a purity above 95% were purchased from Qingdao Heilong Graphite Co., Ltd. Concentrated sulfuric acid (H_2SO_4) and hydrochloric acid (HCl) were purchased from KeLong Chemicals (China). Potassium permanganate ($KMnO_4$) was purchased from Reagent No. 1 Factory of Chengdu Chemical Reagent Co., Ltd. Sodium nitrate ($NaNO_3$) was purchased from Shanghai KeChuang Chemicals Co., Ltd. Hydrogen peroxide (H_2O_2) was purchased from KeLong Chemicals. The materials were used directly without further purification. The graphite oxides were prepared from natural graphite powder by oxidation with $KMnO_4$ in concentrated H_2SO_4 according to Hummer and Offemen's[29] method and as described in our previous article.[30]

All of the polymer materials used in this study were commercially available. PLLA [2002D, *d*-isomer content = 4.3%, weight-average molecular weight = 2.53×10^5 g/mol, melt flow rate = 4–8 g/10 min (190°C/2.16 kg), density = 1.24 g/cm^3] was purchased from Nature-Work. PEG with a molecular weight of 2.0×10^3 g/mol was purchased from KeLong Chemical Reagent Co. (Chengdu, China).

Sample Preparation

First, PEG/GO hybrids were prepared through a solution-mixing method. A solution of GOs in water was obtained by Hummer and Offemen's[29] method, and the concentration of GOs in water was calibrated to 1 mg/mL. After sonication for a long time, the GOs were suspended in water and exfoliated into single-layer GOs as much as possible. Then, the GO solution (1000 mL) was mixed with a water solution containing PEG, and the mixture was stirred overnight. Then, the mixture of PEG and GO was placed in an oven at 80°C for several days to remove water. In this case, a PEG/GO masterbatch with 5 wt % GO was obtained for further blending with PLLA. The PLLA/GO composites were also fabricated by a masterbatch method. First, the water solution of GOs was substituted by a dimethylformamide (DMF) solution with a rotating evaporator at a temperature of 60°C, and the concentration of the GOs in a DMF solution was calibrated to 2.5 mg/mL for further blending. Then, the GO/DMF solution was mixed with the DMF solution containing PLLA and stirred overnight at a temperature of 80°C. The PLLA/GO solution was placed in an oven at 80°C overnight to remove DMF. The PLLA/GO masterbatch with 5 wt % GO was obtained for further blending with PLLA. Finally, the aforementioned PEG/GO and PLLA/GO masterbatches were melt-blended with PLLA at 190°C for 8 min at a screw speed of 90 rpm with a Haake-Rheomix (Haake, Germany). The

corresponding materials with different compositions are shown in Table I.

Characterization

Fourier Transforms Infrared (FTIR) Spectroscopy. FTIR spectroscopy (Nicolet AVATAR 360, Nicolet Instrument Corp.) measurements were conducted in attenuated total reflectance mode at room temperature to detect the surface characteristic of the GOs. The spectra were obtained in the range from 600 to 4000 cm^{-1} with 32 accumulated cycles. The baselines were adopted as they were originally set to be autocorrected. The baseline was determined when the absorbance was zero.

Wide-Angle X-Ray Diffraction (WAXD). Wide-angle X-ray diffractograms of the samples at different annealing times were obtained with a PaNalytical X'Pert PRO diffractometer (The Netherlands) with Ni-filtered Cu Kα radiation. The continuous scanning angle used in this study was from 5 to 40° at 40 kV. To study the annealing effects on the crystallization behavior of the composites, the samples were prepared as follows. The samples were first cooled down from the melt in air and were then annealed at different temperatures [annealing temperature (T_a) = 70 and 100°C] for 4 h.

Scanning Electron Microscopy (SEM). Microscopic morphological observations were conducted on an FEI Inspect F scanning electron microscope (The Netherlands) under an acceleration voltage of 5 kV. To obtain the dispersion state of the GOs in the polymer matrix, the sample was cryofractured in liquid nitrogen and then coated with a gold layer before SEM characterization. Meanwhile, the fractured surface was etched in water at a temperature of 40–60°C for 6 h to remove PEG and identify the morphology of PEG in the PLLA matrix.

Differential Scanning Calorimetry (DSC). To investigate the crystallization behavior of the samples, DSC (Netzsch STA449C Jupiter, Germany) was used. For the DSC measurement, the weight of each sample was about 8 mg. The sample was heated from 0 to 200°C at a heating rate of 10°C/min and maintained at 200°C for 3 min to erase the thermal history. Then, the sample was cooled down to 30°C at a cooling rate of 5°C/min.

The isothermal crystallization and subsequent melting behaviors of the samples were investigated with a PerkinElmer Pyris-1 DSC instrument. For each measurement, the sample was quickly heated to 200°C and maintained at this temperature for 3 min to erase the thermal history; then, the sample was cooled down to a predetermined temperature at a cooling rate of 100°C/min and was maintained at this temperature for a while until the crystallization of the composites was complete. Then, the sample was heated to 200°C at a heating rate of 10°C/min. All of the measurements were carried out under a nitrogen atmosphere.

Polarized Optical Microscopy (POM). A POM instrument (ZERSS, Germany) equipped with a hot stage was used to visualize the microscopic features of the composite film. A sample of about 5 mg was placed between two glass slides and was heated so that it melted completely; then, the sample was pressed to obtain a slice with a thickness of about 20 μm. The slice was first heated to 200°C, and then, the melt was transferred to the hot stage at a temperature of 105°C for isothermal crystallization. All of the samples were maintained at a temperature of 105°C for 20 min, and then, crystalline photos of the samples were recorded with a digital camera.

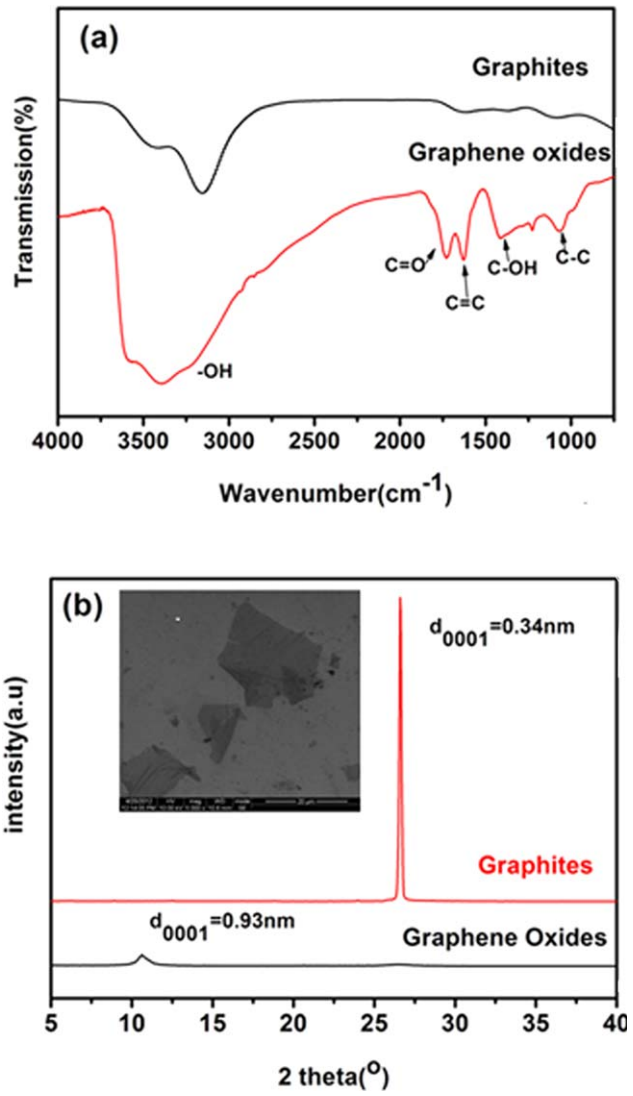

Figure 1. (a) FTIR spectra of the GOs and graphites and (b) XRD spectra of the graphites and GO sheets. The inset shows the typical SEM photos of the GOs. [Color figure can be viewed in the online issue, which is available at wileyonlinelibrary.com.]

RESULTS AND DISCUSSION

GO Nanosheets

The chemical compositions of the GOs and graphites were evaluated by FTIR spectroscopy. As shown in Figure 1(a), the FTIR spectra of the GOs showed several characteristic peaks of various functional groups, including C—O (υ_{C-O} = 1050 cm^{-1}), C—OH (υ_{C-OH} = 1262 cm^{-1}), C=O ($\upsilon_{C=O}$ = 1725 cm^{-1}), and O—H (υ_{O-H} = 3423 cm^{-1}). However, the peaks in the spectra of the graphites were shown to be weak, except the peak at 3423 cm^{-1}, which was assigned to the O—H (υ_{O-H}) of adsorbed water. It was obvious that oxidation made the GOs more polar and active; this was more favorable for the

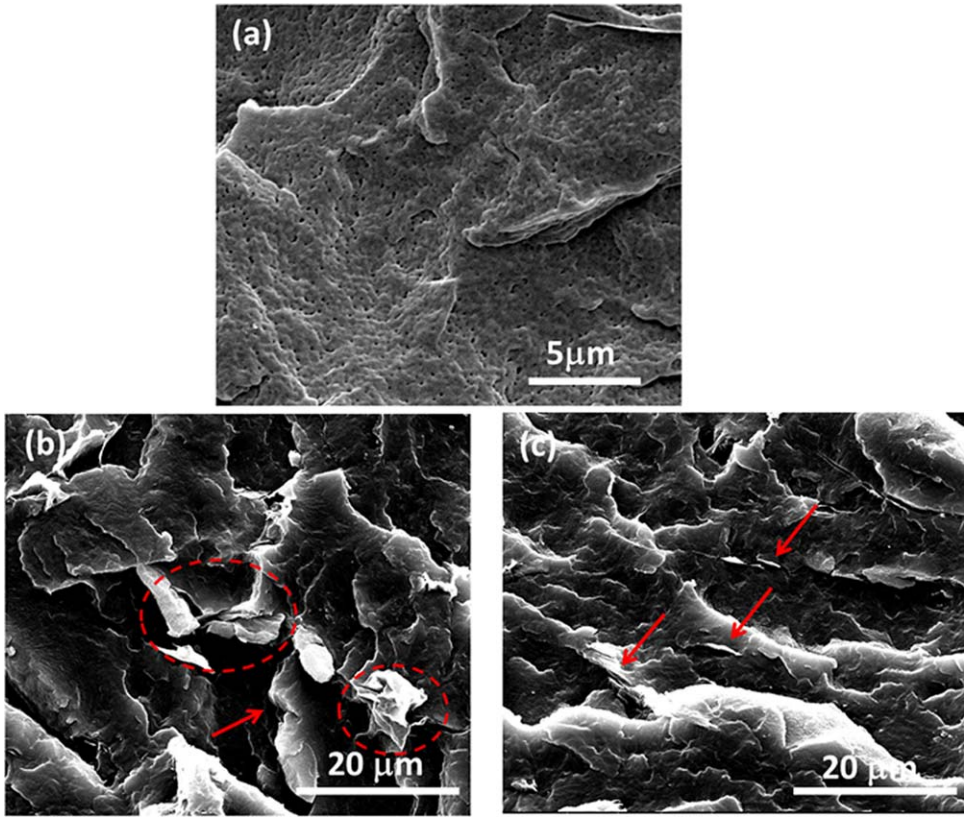

Figure 2. SEM images of the cryofractured surfaces of the (a) PLLA/PEG blend etched by hot water to remove PEG, (b) PLLA/GO composite, and (c) PLLA/PEG/GO composite. [Color figure can be viewed in the online issue, which is available at wileyonlinelibrary.com.]

generation of interactions with polar polymers. On the other hand, the WAXD patterns of the graphites and GOs [Figure 1(b)] showed the differences in the interlayer space; this was a clear indication of the complete transformation from graphites to GOs. In detail, the (001) diffraction peak of the graphites was located at $2\theta = 26.5°$, but it disappeared in the pattern of the GOs. The typical diffraction peak of the GOs was observed at about $2\theta = 10.4°$; this indicated an increase in the interlayer space from 0.34 to 0.93 nm. The variations of the interlayer space indicated that the strong oxidation procedures induced the exfoliation of graphites layers and the transformation from graphites to GOs. The SEM micrograph of the GO sheets prepared by the spin-coating of the GO/water solution is shown in the inset of Figure 1(b). These sheets had an average lateral size of about 10 μm and partially overlapped each other. Buckling of the sheets was evident, particularly in the overlapping region. Obviously, all of the results of FTIR spectroscopy, XRD, and SEM represent a typical nanolayer structure of the GOs obtained by the strong oxidation of graphites.

Morphology of the GOs and PEG in the Polymer Matrix

As is well known, the dispersion of nanofillers in the polymer matrix plays an important role in the improvement of the crystallization behavior. The better the dispersion is, the higher the nucleation efficiency is. Considering this purpose, the PLLA/GO and PLLA/PEG/GO composites were fabricated by the two-step method described in the Experimental section. To further detect the dispersion state of the GOs in polymer matrix, the cryofractured surfaces were observed by SEM, as shown in Figure 2. The PLLA/PEG sample was etched by hot water to remove the PEG phase before SEM characterization, as shown in Figure 2(a). As shown, PEG exhibited a homogeneous distribution in the PLLA matrix, with an average diameter of about 40 nm. This indicated good compatibility between PLLA and PEG as was reported in our previous study.[28] As for PLLA/GO, because of weak interaction between the PLLA and GOs, the GOs could be easily exposed after cryofracturing. We observed that the layerlike GOs were poorly dispersed in the matrix with the stacking and contracting of the GOs layers (as shown by circles and arrows). Sharp interfaces between the PLLA and GOs were also found, as shown in Figure 2(b). On the other hand, we expected that when we relied on the electrostatic repulsion and/or the improved wettability of the GO surfaces by the PEG chains, as described for PEG/oxidized CNT composites,[27,28] a good dispersion of GOs in the PLLA/PEG matrix would be obtained, and interactions between the PLLA and GOs would be enhanced. With the addition of GOs to the PLLA/PEG blend, in the cryofractured surface, the boundary between the polymer and GOs was obscure [as shown in Figure 2(c)], so it was difficult for us to determine the GO distributions. Only the edge of the immersed GO layers could be observed, as shown in Figure 2(c); this indicated better compatibility between the GOs and PLLA. On the other hand, the dispersion of the GOs was improved with the assistance of PEG [as shown in Figure 2(b)].

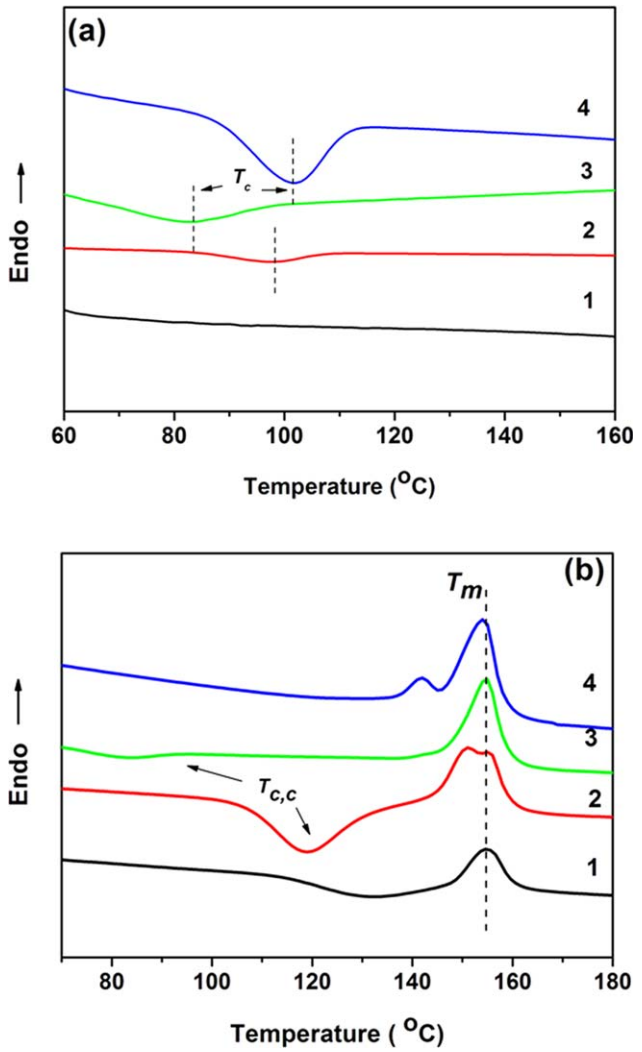

Figure 3. (a) DSC cooling curves showing the nonisothermal crystallization behaviors of different samples at a cooling rate of 5°C/min and (b) DSC heating curves showing the glass-transition, cold-crystallization, and subsequent melting behaviors of the samples after nonisothermal crystallization at a cooling rate of 5°C/min: (1) PLLA, (2) PLLA/GO, (3) PLLA/PEG, and (4) PLLA/PEG/GO. [Color figure can be viewed in the online issue, which is available at wileyonlinelibrary.com.]

Nonisothermal Crystallization Behavior

The nonisothermal crystallization behavior of different samples from the melt state was investigated by DSC. Cooling curves obtained at a cooling rate of 5°C/min for all of the samples are shown in Figure 3(a). For pure PLLA, no crystallization occurred during the cooling process. For the PLLA/GO composite, a weak crystallization peak was found at about 98.2°C because of the heterogeneous nucleation effect of the GOs. For the PLLA/PEG blend, we differentiated an exothermic peak at about 84.0°C, as shown by the arrow; this indicated that PEG promoted the crystallization of PLLA during cooling process by improving the mobility of the PLLA chain segment. However, for the PLLA/PEG/GO composite, a very intense exothermic peak was observed, and the peak temperature increased slightly to 101.6°C. Furthermore, the exothermic peak of the PLLA/PEG/GO composite was shown to be narrower. The onset temperatures of crystallization of the PLLA/PEG blend and PLLA/GO composite were 103 and 109°C, respectively, whereas the onset temperature of crystallization of the PLLA/PEG/GO composite increased up to 113°C. That means that the PLLA/PEG/GO composite could crystallize at a higher temperature with a relatively higher crystallization rate. This was ascribed to two aspects. One was the better dispersion of GOs with assistance of PEG; thus, the nucleation efficiency was enhanced, and this resulted in a higher T_c. The other was that the addition of PEG facilitated the mobility of the chain segment; this resulted in a faster crystalline growth rate. The previous results suggest that the simultaneous presence of the PEG and GOs had a synergistic effect on the crystallization of PLLA.

The corresponding heating curves after nonisothermal crystallization are shown in Figure 3(b), and the corresponding characteristics are listed in Table II. The crystallinity was calculated with the following equation:

$$X_c = \frac{\Delta H_m - \Delta H_{c,c}}{\Delta H_m^0} \times 100\%$$

where ΔH_m is the exothermic enthalpy of melting, $\Delta H_{c,c}$ is the enthalpy of cold crystallization, and $\Delta H_m^0 = 93\,J/g$ is the exothermic enthalpy of melting of PLLA with 100% crystallinity.[31]

For pure PLLA, we observed the cold-crystallization temperature ($T_{c,c}$) at 128.4°C and the melting temperature (T_m) at 154.9°C. It was proven that the melting behavior of PLLA observed in Figure 3(b) was due to the fusion of crystallites formed during the DSC heating process through cold crystallization. Cold crystallization occurred at a relatively high temperature (130°C), which could provide enough chain mobility for PLLA; therefore, the PLLA lamellar was more perfect with a homogeneous distribution, and this resulted in only one fusion peak.[32] For the PLLA/GO composite, $T_{c,c}$ decreased down to 118.9°C; this indicated that the GOs also promoted the cold crystallization of PLLA during the heating process; this was possibly due to the heterogeneous nucleation effect of the GOs. However, a low T_c may have prevented the perfection of the lamellar structure, and double melting peaks were observed for the PLLA/GO composite. A very intense exothermic peak was observed for the PLLA/PEG blend, and a weak peak attributed to cold crystallization was observed at 82.3°C. This occurred because the enhanced mobility of PLLA originating from the plasticizing effect of PEG promoted the cold crystallization of PLLA. PLLA partially crystallized during the cooling process, as

Table II. $T_{c,c}$, T_m, and X_c Values of the Samples after Nonisothermal Crystallization

	$T_{c,c}$ (°C)	T_m (°C)	T_c (°C)	X_c (%)
PLA	128.4	154.9	—	—
PLA/GO	118.9	151.1/155.6	98.2	—
PLA/PEG	82.3	142.3/154.7	84.0	20.3
PLA/PEG/GO	—	141.8/154.3	101.6	29.4

PLA, poly(lactic acid).

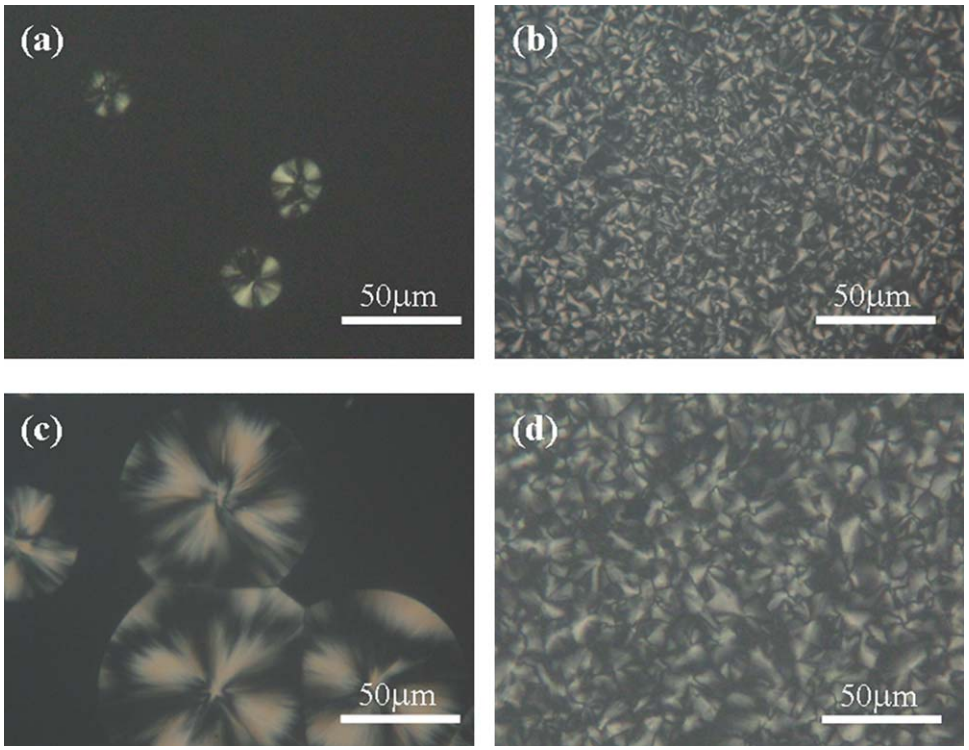

Figure 4. POM images showing the isothermal crystallization morphologies obtained after isothermal crystallization at 105°C for 20 min: (a) PLLA, (b) PLLA/GO, (c) PLLA/PEG, and (d) PLLA/PEG/GO with 0.5 wt % GOs. [Color figure can be viewed in the online issue, which is available at wileyonlinelibrary.com.]

shown in the cooling curve, and the amount of cold-crystallized PLLA was less than that of the PLLA/GO composite. In this case, a weak cold-crystallization peak was observed. On the other hand, PEG could enhance the chain mobility and facilitate the perfection of crystalline structure. Therefore, two endothermic peaks were inconspicuous, and more perfect lamella, indicated by only one melting peak with higher temperatures, were obtained for the PLLA/PEG blend. For the PLLA/PEG/GO composite, there were only intense melting peaks in the heating curves; this indicated that the PLLA completed crystallization during cooling, and no further crystallization occurred during heating. There were two endothermic peaks at 141.8 and 154.3°C. The former was mainly ascribed to the fusion of those lamellae with smaller thicknesses or some imperfect lamellae, and the latter may have resulted from the partial melt–recrystallization–melt of some primary crystallites or the fusion of more perfect lamella. Correspondingly, the crystallinity of the PLLA/PEG/GO composite was greatly increased compared with pure PLLA. As we concluded from the nonisothermal crystallization behavior, the effectiveness of the PEG and/or GO was sufficient to promote crystallization of PLLA.

Isothermal Crystallization Behavior

The crystallization morphologies obtained after isothermal crystallization at 105°C are shown in Figure 4. All photos were taken with a crystallization time of 20 min. Under these conditions, pure PLLA [Figure 4(a)] showed typical morphologies of spherulites, and the diameters of the spherulites were about 20–30 μm. Much smaller spherulites or tiny crystallites were observed for the PLLA/GO composite [Figure 4(b)]; this indicated that GOs acted as efficient nucleation agents and increased the density of the nucleus in the PLLA matrix. For the PLLA/PEG blend shown in Figure 4(c), we observed that the PLLA spherulites were about 50–60 μm, whereas the nucleation density remained unchanged compared with pure PLLA. This was due to the enhanced chain mobility of the PLLA segments induced by the plasticizer PEG; this may have facilitated the growth of the spherulites. Obviously, the individual role of the PEG or GOs was significant for its own role. For the PLLA/PEG/GO ternary composite, many more PLLA spherulites compared with PLLA/PEG composites were clearly observed, and spherulites with moderately increased sizes compared with the PLLA/GO composites were found, as shown in Figure 4(d). Compared with pure PLLA, the addition of both GOs and PEG not only increased the density of the nucleus but also accelerated the growth of the PLLA spherulites. In conclusion, the GOs and PEG had a synergistic effect on the crystallization behavior of PLLA. Finally, this resulted in an increased nucleation density and growth rate of PLLA crystallization compared with pure PLLA. According to Li et al.'s[23] study, 2D GNSs exhibited strong nucleation ability; this could be attributed to surface-induced conformational order, beginning with the —(COC + CH_3) interchain interactions.

The isothermal crystallization kinetics of the samples were also investigated to obtain a better understanding of the synergistic effect of the GOs and PEG on the crystallization behavior of the PLLA matrix. Figure 5(a) shows the isothermal crystallization

Applied Polymer SCIENCE

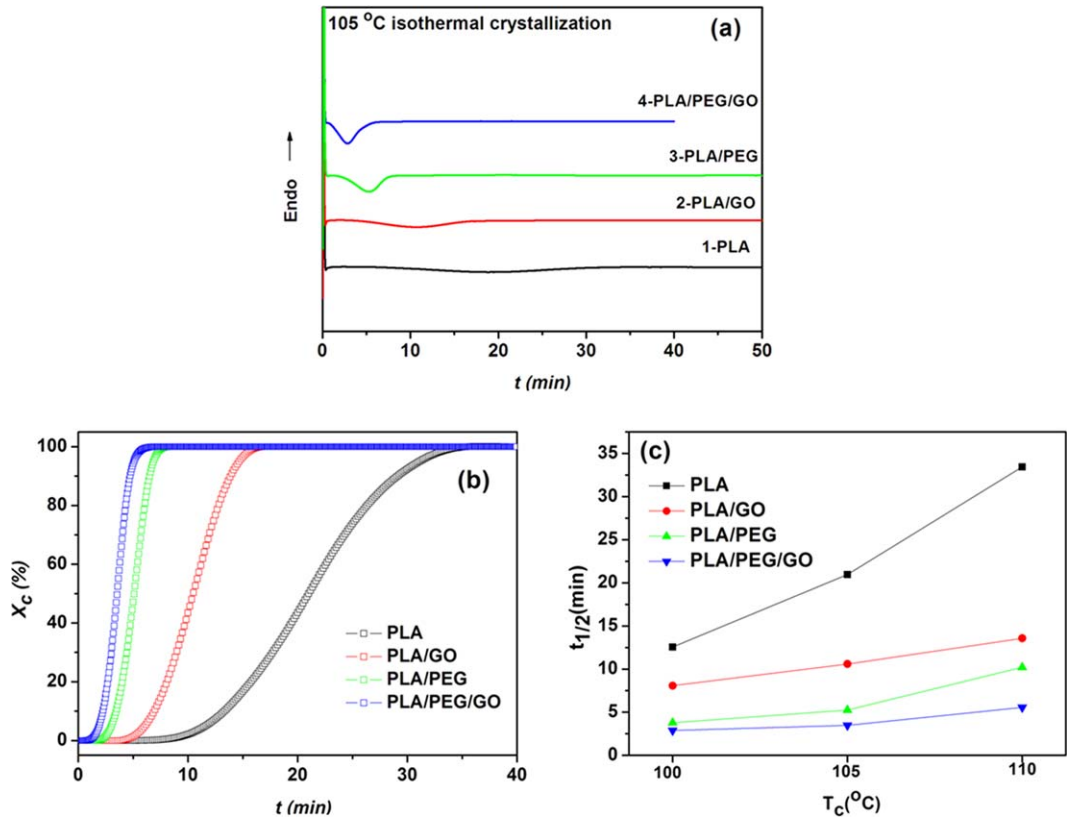

Figure 5. Isothermal crystallization behaviors of the samples: (a) DSC curves of the samples crystallized at 105°C, (b) $X(t)$ versus crystallization time of the samples at an isothermal crystallization of 105°C, and (c) $t_{1/2}$ versus T_c curves. [Color figure can be viewed in the online issue, which is available at wileyonlinelibrary.com.]

curves of the samples that crystallized at 105°C. For a direct observation, pure PLLA showed a broad exothermic peak; this indicated the slowest crystallization process among all of the samples, whereas for the PLLA/PEG and PLLA/GO composite, the crystallization time was obviously shortened compared with that of PLLA. Most important was that the peak of PLLA/PEG/GO composite was much narrower; this indicated that it took the least time to complete the crystallization among all of the samples. As we know, $t_{1/2}$, defined as the time required to reach 50% of the complete crystallization, is an important parameter in describing the overall crystallization rate. The higher $t_{1/2}$ is, the slower the crystallization rate is. Therefore, the comparison of the relative X_c evolution curves of all of the samples at a T_c of 105°C with enough crystallization time is shown in Figure 5(b). Apparently, under these conditions, the PLLA/PEG/GO composite crystallized faster than PLLA/PEG and PLLA/GO. For a more clear description of the isothermal crystallization behavior, the $t_{1/2}$ values of PLLA, PLLA/PEG, PLLA/GO, and PLLA/PEG/GO were plotted against the T_c values, as shown in Figure 5(c). As shown, the overall crystallization rate decreased with increasing T_c for each sample. Compared with pure PLLA, the composite containing only PEG or GOs showed an acceleration effect of crystallization. The former was due to the enhanced chain segment mobility, and the latter resulted from the heterogeneous nucleation effect of the nanofiller for polymer crystallization; this has been widely observed in polymer/graphene[20–25] and PLLA/nanofiller[33,34] composites. For the ternary composite, the simultaneous introduction of both PEG and GOs shortened the crystallization time compared with the composite containing only PEG or GOs. When the samples crystallized at higher temperatures, the synergistic effect was more significant. For example, when the samples crystallized at a higher temperature of 105°C, $t_{1/2}$ was reduced from 32 min for PLLA to 5.3 min for the PLLA/PEG/GO composite.

The Avrami equation[35–37] was used to study the crystallization kinetics of the samples as follows:

$$1-X(t)=\exp(-Kt^n)$$

where $X(t)$ is the relative crystallinity, which is calculated as the ratio of the heat of fusion at time t to the total heat of fusion of the whole crystallization process; n is the Avrami exponent, which is dependent on the type of nucleation and the growth mechanism during the crystallization; and K is the crystallization rate parameter. Points were collected between $X(t)$ values of 0 and 100%. According to the Avrami equation, one formula can be obtained as follows:

$$\log\left[-\ln\left(1-X_t\right)\right]=n\log\ t+\log\ K$$

Generally speaking, the plot of $\log[-\ln(1-X_t)]$ versus $\log\ t$ is a straight line, the slope of the line is n, and the intercept with the ordinate yields $\log K$. On the basis of the previous formula, the parameters of the isothermal crystallization kinetics were

Table III. Isothermal Crystallization Parameters of the PLLA Composites

Sample	T_c (°C)	log k	n	$t_{1/2}$(min)
PLA	100	−3.50	3.01	12.6
	105	−3.68	2.57	22.4
	110	−4.77	2.89	36.5
PLA/GO	100	−2.38	2.52	8.1
	105	−2.47	2.48	10.6
	110	−2.82	2.39	12.6
PLA/PEG	100	−2.02	3.15	3.8
	105	−2.16	2.72	5.2
	110	−2.69	2.46	10.2
PLA/PEG/GO	100	−1.41	2.62	2.9
	105	−1.64	2.64	3.5
	110	−1.90	2.45	5.6

PLA, poly(lactic acid).

calculated and are shown in Table III. For all of the samples in the temperature region studied, log K decreased with increasing T_c; this indicated that the crystallization rate decreased at higher T_c values. At the same T_c, compared with pure PLLA, the log K values of the PLLA/PEG, PLLA/GO, and PLLA/PEG/GO composites showed an obvious increase, and the disparity among the three samples was substantial.

The n value typically reveals the growth dimension of the polymer. For all samples, n ranged from 2 to 3; this means that spherulite growth arose from an athermal heterogeneous nucleation. For samples containing GOs, n decreased slightly compared with PLLA and PLLA/PEG. A general trend can normally be obtained when one compares the n of polymer nanocomposites with those of a pure polymer. For example, it was reported that the addition of a small amount of clay resulted in an n value of PE that decreased to 1.6.[38] Li et al.[26] investigated RGO-induced PE crystallization in solution and nanocomposites, and they concluded that the addition of RGO brought about an n value decrease from 2.5 to 1.93 when 0.04 vol % RGO was incorporated into the PE matrix. This was the reason numerous spherulites grew at or near the graphene surface, impinged with each other at a relatively early stage of crystallization, and formed a quasi-2D layer of spherulites. Therefore, the observed n decreased. In our study, the GOs dominated the heterogeneous nucleation of PLLA, and this also matched well the 2D layer nucleation capability of the GOs.

Effect of Annealing on the Crystallization Behavior

As we know, to improve the crystallization of PLLA, annealing as a new methodology has been applied to further develop the crystallization of PLLA and has led to increases in the crystallinity and the improvement of the physical properties of PLLA. In this study, to further investigate the synergistic effects of GOs

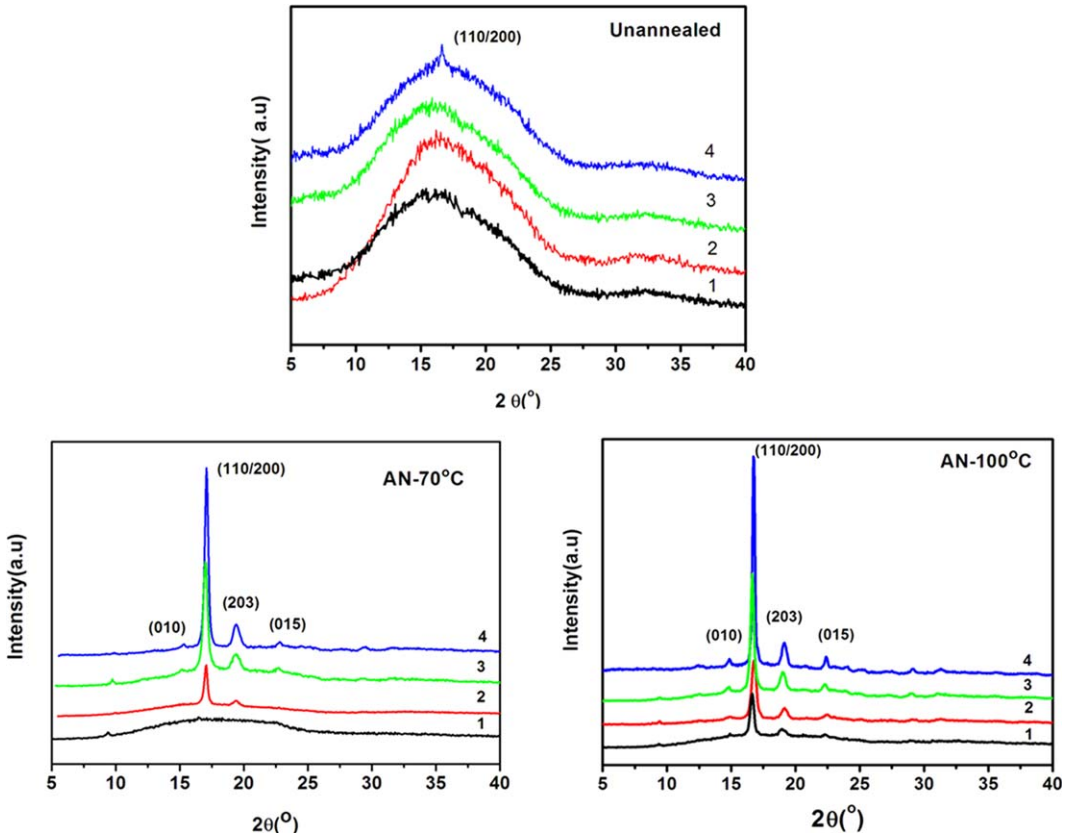

Figure 6. WAXD profiles of samples obtained after they were annealed for 4 h at different temperatures as indicated in the graphs: (1) PLLA, (2) PLLA/GO, (3) PLLA/PEG, and (4) PLLA/PEG/GO. The annealed samples were defined as AN-x, where x indicated the annealing temperatures. For example, AN-70°C mean the samples annealed at 70°C. [Color figure can be viewed in the online issue, which is available at wileyonlinelibrary.com.]

Applied Polymer SCIENCE

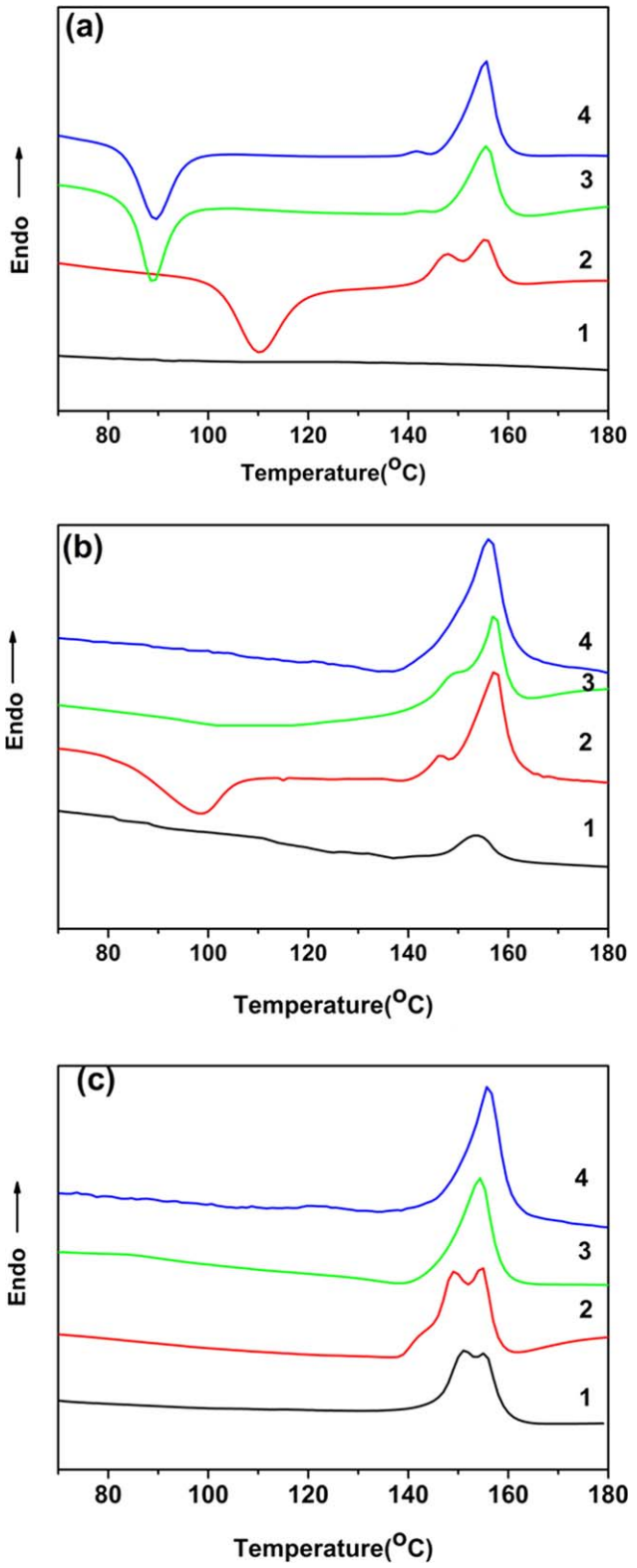

Figure 7. DSC heating curves showing the different glass-transition, cold-crystallization, and subsequent melting behaviors of samples obtained before and after they were annealed for 4 h at different temperatures: (a) unannealed samples, (b) samples annealed at 70°C, and (c) samples annealed at 100°C: (1) PLLA, (2) PLLA/GO, (3) PLLA/PEG, and (4) PLLA/PEG/GO. [Color figure can be viewed in the online issue, which is available at wileyonlinelibrary.com.]

and PEG on PLLA crystallization, melt-quenched samples were annealed at different temperatures for 4 h. The annealed and unannealed samples were characterized by WAXD analysis and DSC measurements. The crystalline structures of the samples were first examined by WAXD, and the results are shown in Figure 6. For the melt-quenched samples without annealing treatment, no visible diffraction peak attributed to the crystalline structure was detected for the pure PLLA, PLLA/PEG, and PLLA/GO samples; this indicated that the three samples were completely amorphous or that the crystallites were so tiny that crystalline structures could not be traced by WAXD. Interestingly, the spectrum of the PLLA/PEG/GO composite exhibited a small visible peak at $2\theta = 16.7°$, which was assigned to the diffraction peak of the (110/200) plane and suggested an enhanced crystallization ability over those of the other samples. Even though the cooling rate was high enough, the synergistic effect was also significant. This was different from the PLLA/PEG/CNTs composite we studied previously[28] and may have been caused by the more extensive 2D-layer nucleation sites of the GOs. After being annealing at a lower T_a (70°C), all of the samples exhibited crystalline diffraction peaks of the (110/200) plane at $2\theta = 16.7°$ and the (203) plane at $2\theta = 19.1°$. New diffraction peaks of the (010) plane at $2\theta = 14.7°$ and the (015) plane at $2\theta = 22.3°$ were found for the PLLA/PEG and PLLA/PEG/GO samples. This phenomenon further proved the synergistic effects of the PEG and GOs on the secondary crystallization of PLLA during annealing. With increasing T_a, all of the featured peaks of PLLA were observed for all of the samples, and the role of PEG and/or GOs seemed to be inconspicuous. The reason for this phenomenon was that because of the long annealing time of 4 h, the crystallizations of all of the samples were completely finished. In this case, for the crystallization behavior, the distinctions among all of the samples were not evident.

Figure 7 shows the DSC curves of the samples, and their characteristic parameters are listed in Table IV. For the PLLA/GO composite, the incorporation of GOs led to the occurrence of cold crystallization at 110.3°C because of the increased nucleation density compared with pure PLLA. As for the PLLA/PEG blends, $T_{c,c}$ decreased to 89.2°C because of the easier mobility of the chain segments induced by the plasticizer effect of PEG. $T_{c,c}$ of the PLLA/PEG/GO composite also decreased to 88.4°C and was close to that of the PLLA/PEG samples. Correspondingly, the T_m's of all of the samples showed multiple melting peaks. It has been reported that multiple melting peaks can be ascribed to two mechanisms: one is the α'–α transition occurring during heating, and the other is melt–recrystallization–melt behaviors. The results obtained from the WAXD profiles proved that only the α form was present in all of the samples. Thus, we deduced that the endothermic peak observed at low temperatures was assigned to the melting of some primary crystallites or the fusion of lamella with relatively small thicknesses. The peak at high temperatures was attributed to the melting of more perfect or recrystallized crystals.[39] On the other hand, the resulting absence of crystallinity in Table IV indicated that the endothermic melting peaks assigned to the fusion of PLLA crystallites may have possibly arisen from the cold-crystallization process during heating. Although the addition of PEG resulted

Table IV. $T_{c,c}$, T_m, and X_c Values of the Samples after Annealing at Different Temperatures for 4 h

		PLA	PLA/GO	PLA/PEG	PLA/PEG/GO
$T_{c,c}$ (°C)	Unannealed	—	110.3	89.2	88.7
	70°C	114.0	98.4	—	—
	100°C	—	—	—	—
T_m (°C)	Unannealed	—	147.4/155.2	142.9/155.3	141.3/155.3
	70°C	153.8	145.8/157.3	148.2/157.1	156.4
	100°C	151.1/155.1	148.8/155.3	155.1	156.0
X_c (%)	Unannealed	—	—	—	11.8
	70°C	—	14.2	16.4	20.1
	100°C	9.8	19.7	18.4	21.6

PLA, poly(lactic acid).

in a decrease of $T_{c,c}$, the plasticizing effect endowed enough chain mobility for PLLA; this was more favorable for the perfection of the lamellar structure. Therefore, the amount of perfect lamella of PLLA/PEG and PLLA/PEG/GO was greater than that of the PLLA/GO composite. On the other hand, the enhanced nucleation density in the 2D planar geometry of the GOs may have prevented the perfection of the PLLA lamella because of the impingements of lamella; finally, the lamellar reorganization behavior revealed by double melting peaks was more significant compared with those in the PLLA/PEG blend and PLLA/PEG/GO composite. It was interesting to find that the fusion of the PLLA crystallites did not totally originate from cold crystallization, and an X_c of 11.8% was obtained. This means that even though the cooling rate of the quenched sample was high enough, the simultaneous addition of PEG and GOs made a positive impact on the promotion of PLLA crystallization; this also matched the results of WAXD well.

As shown in Figure 7(b), when T_a was 70°C, which was slightly higher than the glass-transition temperature, the cold temperature of pure PLLA was not visible on the heating curve, but a weak fusion peak was observed, which indicated that PLLA partially crystallized during the heating process. In this case, the increased crystallinity was found for pure PLLA. As for the PLLA/GO composite, $T_{c,c}$ of the annealed sample decreased to 98.4°C; this was ascribed to the increased amount of nucleus formed during the annealing process. No cold-crystallization behavior occurred for the PLLA/PEG and PLLA/PEG/GO composites; this suggested that a cold crystallization was completed during the annealing process because of the plasticizing effect of PEG. Furthermore, the T_a of 100°C was high enough that the mobility of the polymer chain segments was enhanced and the crystallization of PLLA was completed during the annealing process. As a result, the cold-crystallization phenomenon during the heating process disappeared, as shown in Figure 7(c). The melting peaks were ascribed to the fusion of crystallites formed during the annealing process rather than cold crystallization that occurred during the DSC heating process. Furthermore, PEG may have enhanced the chain mobility of PLLA and facilitated the lamellar packing and perfection of the crystalline structure of PLLA. Therefore, only one fusion peak with a relatively higher T_m was found in the PLLA/PEG blend and PLLA/PEG/GO composite. As for PLLA/GO, it was easy for the increased nucleation density to prevent the formation of PLLA spherulites with perfect lamella, as discussed previously, and we observed multiple melting peaks in the heating curve. With increasing T_a, the crystallinities of all of the samples increased, and the increased maximum was for PLLA/PEG/GO. This indicated a synergistic effect of the PEG and GOs on annealing-induced crystallization.

In this study, we focused on the crystallization behaviors of PLLA and its related composites. Actually, a synergistic effect of PEG and GOs on the crystallization behavior also played an important role in improvements in the mechanical properties of PLLA. For example, the elastic modulus increased from 1562 MPa for the pure PLLA to 1745 MPa for the PLLA/PEG/GO ternary composites. This also motivated us to lead a further study on the properties of PLLA/PEG/GO. In this case, a systematic investigation into the rheological properties, mechanical properties, and crystallization behavior will be undertaken to establish the relationship between the structure and properties in a future work.

CONCLUSIONS

The crystallization behavior of PLLA blended with PEG and/or GOs was investigated under different thermal conditions, such as nonisothermal crystallization, isothermal crystallization, and crystallization behaviors during annealing. The results show that GOs functioned as a 2D-layer nucleation agent to improve the nucleation density and PEG functioned as a plasticizer to enhance the mobility of the chain segments of PLLA. When PEG and GOs were incorporated into the PLLA matrix simultaneously, the PEG and GOs had synergistic effects on the crystallization of PLLA; this resulted in an increased crystallization rate and higher crystallinity. In this study, we explored a new strategy to govern the PLLA product with an improved crystalline structure and also provided GOs with a new application field.

ACKNOWLEDGMENTS

The authors thank the National Natural Science Foundation of China (contract grant numbers 51173151, 50973090, and 51203129), the Fundamental Research Funds for the Central

Universities (contract grant numbers SWJTU11CX142, SWJTU11ZT10, and SWJTU12CX010), and the Opening Project of State Key Laboratory of Polymer Materials Engineering, Sichuan University (contract grant number KF201309) for financial support.

REFERENCES

1. Taylor, M. S.; Daniel, A. U.; Andriano, K. P.; Heller, J. J. *Appl. Biomater.* **1994**, *5*, 151.
2. Drumright, R. E.; Gruber, P. R.; Henton, D. E. *Adv. Mater.* **2000**, *12*, 1841.
3. Tsyhu, H.; Ikada, Y. *Polymer.* **1995**, *36*, 2709.
4. Pluta, M. *Polymer.* **2004**, *45*, 8239.
5. Kulinski, Z.; Piorkowska, E. *Polymer* **2005**, *46*, 10290.
6. Qiu, Z. B.; Li, S. Z. *Ind. Eng. Chem. Res.* **2011**, *50*, 12299.
7. Bai, H. W.; Zhang, W.; Deng, H.; Zhang, Q.; Fu, Q. *Macromolecules* **2011**, *44*, 1233.
8. Wang, L. Y.; Jing, X. B.; Cheng, H. B.; Hu, X. L.; Yang, L. X.; Huang, Y. B. *Ind. Eng. Chem. Res.* **2012**, *51*, 10088.
9. Urayama, H.; Kannamori, K.; Kimura, Y. *Macromol. Mater. Eng.* **2003**, *288*, 137.
10. Bai, H. W.; Xiu, H.; Gao, J.; Deng, H.; Zhang, Q.; Yang, M. B.; Fu, Q. *Am. Chem. Soc. Appl. Mater. Interface* **2012**, *4*, 897.
11. Sinclair, R. G. J. *Macromol. Sci. Pure Appl. Chem.* **1996**, *33*, 583.
12. Nijenhuis, A. J.; Colstee, E.; Grijpma, D. W.; Pennings, A. J. *Polymer* **1996**, *37*, 5849.
13. Martin, O.; Averous, L. *Polymer* **2001**, *42*, 6209.
14. Ohikohi, I.; Abe, H.; Doi, Y. *Polymer* **2000**, *41*, 5985.
15. Xu, Z. H.; Niu, Y. H.; Wang, Z. G.; Li, H.; Yang, L.; Qiu, J.; Wang, H. *Am. Chem. Soc. Appl. Mater. Interfaces* **2011**, *3*, 3744.
16. Brezezinski, M.; Bogustawska, M.; Mosnacek, J.; Biela, T. *Macromolecules* **2012**, *45*, 8714.
17. Ray, S. S.; Yamada, K.; Okamoto, M.; Uede, K. *Nano Lett.* **2002**, *2*, 1093.
18. Wu, D.; Wu, J.; Wu, L.; Xu, B.; Zhang, Y.; Zhang, M. J. *Polym. Sci. Part B: Polym. Phys.* **2007**, *45*, 1100.
19. Krikorian, V.; Pochan, D. J. *Macromolecules* **2005**, *38*, 6520.
20. Samir, A. S. A.; Allion, F.; Dufresne, A. *Biomacromolecules* **2005**, *6*, 612.
21. Cai, D. Y.; Song, M. J. *Mater. Chem.* **2010**, *20*, 1906.
22. Liang, J.; Huang, Y.; Zhang, L.; Wang, Y.; Ma, Y.; Guo, T.; Chen, Y. *Adv. Funct. Mater.* **2009**, *19*, 2297.
23. Xu, J. Z.; Chen, T.; Yang, C. L.; Li, Z. M.; Mao, Y. M.; Zeng, B. Q.; Hsiao, B. S. *Macromolecules* **2010**, *43*, 5000.
24. Gao, Y. W.; Feng, J. C.; Wu, P. Y. *Carbon* **2010**, *48*, 3834.
25. Bao, C. L.; Song, L.; Xing, W. Y.; Yuan, B. H.; Wilkie, C. A.; Huang, J. L.; Guo, Y. Q.; Hu, Y. J. *Mater. Chem.* **2012**, *22*, 6088.
26. Cheng, S.; Chen, X.; Hsusan, G.; Li, Y. C. *Macromolecules* **2011**, *50*, 34.
27. Linda, V.; Gad, M.; Wagner, H. D. *Adv. Funct. Mater.* **2006**, *16*, 357.
28. Li, Y. L.; Li, X. X.; Xiang, F. M.; Huang, T.; Wang, Y.; Wu, J.; Zhou, Z. W. *Polym. Adv. Technol.* **2011**, *22*, 1959.
29. Hummer, W. S.; Offemen, R. E. J. *Am. Chem. Soc.* **1958**, *80*, 1339.
30. Yang, J.; Feng, C.; Dai, J.; Zhang, N.; Huang, T.; Wang, Y. *Polym. Int.* [Online early access]. DOI: 10.1002/pi.4396. Published Online: Nov 6, 2012. http://onlinelibrary.wiley.com/doi/10.1002/pi.4396/abstract. Accessed on May 21, 2013.
31. Fisher, E.; Sterzel, H. J.; Wegner, G. Z. Z. *Kolloid Polym.* **1973**, *251*, 980.
32. Shi, Y.; Shao, L.; Yang, J.; Huang, T.; Wang, Y.; Zhang, N.; Wang, Y. *Polym. Adv. Technol.* **2013**, *24*, 42.
33. Nam, J. Y.; Ray, S.; Okamoto, M. *Macromolecules.* **2003**, *36*, 7126.
34. Bourbigot, S.; Fontaine, G. *Polym. Chem.* **2010**, *45*, 1413.
35. Avrami, M. J. *Chem. Phys.* **1939**, *7*, 1103.
36. Avrami, M. J. *Chem. Phys.* **1940**, *8*, 212.
37. Avrami, M. J. *Chem. Phys.* **1941**, *9*, 177.
38. Haggenmueller, R.; Fisher, J. E.; Winey, K. I. *Macromolecules* **2006**, *39*, 2964.
39. Pan, P.; Zhu, B.; Kai, W.; Dong, T.; Inoue, Y. *Macromolecules* **2008**, *41*, 4296.